

# All-carbon nanotube-based junction with virtual source and drain of carbon nanotubes by *in situ* one-step process for practical integrated nanoelectronics

Yun-Hi Lee,<sup>a)</sup> Je-Min Yoo, and Jong-Hee Lee

National Research Laboratory, Korea University, Seoul 136-713, Korea and Nano Device and Physics Laboratory, Korea University, Seoul 136-713, Korea

B. K. Ju

College of Electrical and Electronics Engineering, Korea University, Seoul 136-713, Korea

(Received 5 April 2006; accepted 25 October 2006; published online 11 December 2006)

The authors propose a suspended *in situ* lateral grown all-carbon nanotube-based junction and report on the dc carrying behaviors of the carbon nanotube junction, especially with and after UV exposure. Also, the release of carriers of the junctions was studied by capacitance ( $C$ ) measurements with ac excitation. The designed diluted magnetic impurity doped oxide film was adopted as catalyst in the fabrication of the junction. The suspended nanotube channel showed ambipolar function and almost the same low barrier height for the holes and electrons, which was determined by  $I$ - $T(K)$  measurements. Subsequent measurements on the channel treated by low intensity UV resulted in a highly conductive channel with high current carrying behavior. Both their *junction structure* and *analogy* between dc  $I$ - $V$  and capacitance can be applied to develop a practical and accessible system for forming reproducible integrated nanoelectronic junctions as well as to accelerate the realization of all low dimensional molecular devices. © 2006 American Institute of Physics.

[DOI: 10.1063/1.2403186]

The switching and transport properties of nanotube field effect transistors (FETs) have been explained by the Schottky barrier modulation model, whose behavior is dominated by the contact barrier height between the nanotube and a metal.<sup>1-12</sup> Therefore, one can expect that Schottky barriers will also allow the nanotube devices to behave as  $p$ -,  $n$ -, or ambipolar FETs when the band lineup at the contacts is controlled approximately. Also, recent reports have suggested that the contact properties of the electrode metal-carbon nanotube (CNT) junction is dominated not only by the work function of the metal but also by the interfacial dipole.<sup>8</sup>

In this letter, we propose and fabricate nanotube FETs by using CNT as the contact electrodes. The charge density of the dipole at the contact interface was decreased by adopting material continuity and the change of the contact properties due to external ambient effect such as oxygen, etc., was prevented. The electrical transport properties of the CNT electrode-channel CNT-CNT electrode of the fabricated three terminal junctions are discussed for the first time with respect to dc  $I$ - $V$ - $T(K)$  and capacitance ( $C$ )-frequency ( $f$ )-bias ( $V_{ds}$ ) measurements. High current carrying<sup>13</sup> all-CNT-based junctions were constructed by suspended *in situ* lateral growth for the first time. We used the one-step process method to grow suspended CNT between photolithographically defined patterned electrodes.<sup>14,15</sup>

The typical scanning electron microscope image of a typical all-CNT-based junction is shown in Fig. 1. Our direct lateral growth method used normally patterned catalytic electrodes as shown in the inset of Fig. 1. The suspended  $\sim 2.5$   $\mu\text{m}$  long CNT shows a well-crossing bridge, and the CNT electrodes consist of an entangled CNT network. The linear relationship of the  $I$  and  $V_{sd}$  at a low drain-source bias

indicated the formation of a fairly good Ohmic contact of the entangled CNT network electrodes to the CNT bridge. Figures 1(a) and 1(b) show the typical drain current versus drain-source voltage characteristics of a CNT electrode pad and CNT channel for the same device at different values of the gate voltage ( $V_g$ ), respectively. Several noticeable observations can be made from this figure: (1) the electrode CNT shows good current carrying capacity even under very small  $V_{sd}$  of 7 mV and (2) the suspended CNT channel is semiconducting, showing gate coupling as well as ohmic properties in the small  $V_{sd}$  region, as shown in inset. One of the distinct differences between the CNT electrode and the CNT channel was the conduction properties; the CNT electrode showed high conduction<sup>13</sup> of 2 k $\Omega$  and CNT channel of 1500 k $\Omega$ . The  $I$ - $V_{sd}$  and  $dI/dV$ - $V_{sd}$  of the CNT channel, which were measured at different temperatures down to 8 K, showed increasingly nonlinear behavior with decrease in temperature as shown in (c). Figure 1(d) shows the current versus temperature characteristics, which can be used to estimate barrier height from  $I$ - $V_{sd}$  taken in the range of 8–297 K, with  $V_g = -8, 0, +8$  V, i.e., in the strong hole and electron accumulation regions. Arrhenius plot of the channel current ( $I$ ) shows the thermionic above 84 K and tunnel conduction below about 84 K and the drastic change of the shapes of the curves.<sup>16</sup> At a lower temperature, the transport via thermally activated conduction was effectively suppressed and the carrier conduction was dominated by tunneling. The barrier heights for hole and electron injections were 211 and 223 meV in the thermally activated conduction region, respectively. The result suggests the existence of the Schottky barrier at the CNT-based electrode/CNT-based channel contact, and furthermore/the nearly symmetrical barrier heights suggest that the Fermi level at the electrode/channel lines up close to the middle of the gap of the suspended CNT.

Figures 2(a)–2(c) show the transfer characteristics ( $I$  vs  $V_g$ ) of a typical CNT electrode and a suspended CNT chan-

<sup>a)</sup> Author to whom correspondence should be addressed; electronic mail: yh-lee@korea.ac.kr

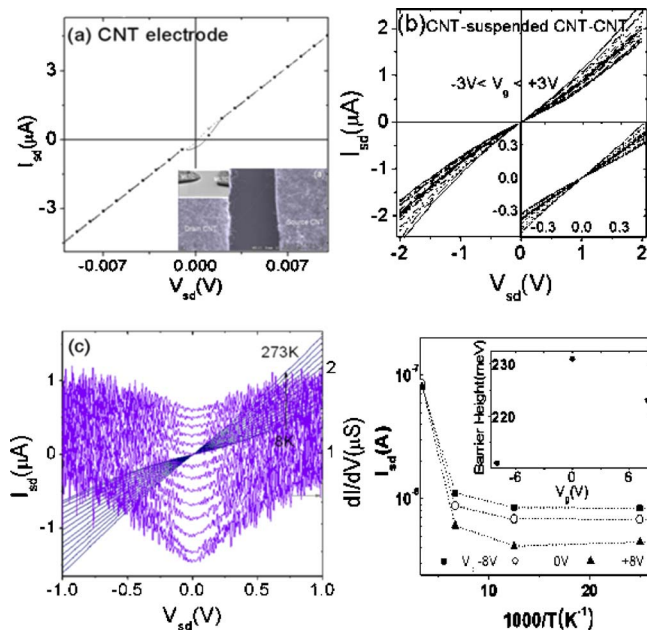


FIG. 1. (Color online)  $I$ - $V$  characteristics of a typical all-carbon nanotube-based three terminal junction made by direct *in situ* suspended growth. (a)  $I$ - $V_{sd}$  characteristics of each CNT electrode. To measure this current, two probes were laid on an entangled CNT sheet, acting as drain and source electrodes, respectively. (b) CNT channel current vs drain bias with  $V_g$ . The inset figure shows a patterned layered catalyst for lateral bridging of CNT. (c) Temperature dependent change of  $I$  and appearance of Coulomb gap in the low temperature regime. Doped-Si substrate was used as gate electrode.

nel during and after UV exposure for the same channel CNT device. In CNT as an electrode, as shown in (a), typical ambipolar characteristics were observed in the low  $V_{sd}$  regime and increasing  $V_{ds}$  resulted in  $P$ -type characteristics. More importantly, the current in the CNT electrodes decreases nearly steplike in the positive  $V_g$  region; this result suggests that the peeling breakdown of metallic CNTs within the CNT electrode occurred successively under UV.

On the other hand, CNT bridge as a channel carrying current of  $16 \mu A/2 \mu m$  showed also ambipolar characteristics, although it still maintained  $P$ -type dominant conduction, whose amount was reduced during UV exposure without significant shift of the threshold voltage of switching. For the result in Fig. 2(c), we can include both effects such as the photodesorption of oxygen, which changes the transport current by altering the band lineup at the Schottky barriers, resulting in the decrease of channel current during UV exposure.<sup>17</sup> and cleaning surface of CNT. That is, an increase of conductance after the exposure can be explained due to both the hole doping effect of oxygen on the long CNT channel and the removal of amorphous layer of the CNT channel, which increased the current level.<sup>18</sup>

Finally, we examined the aging properties of the channel for a few days without break for a large negative  $V_g$  under average ambient humidity of  $\sim 50\%$ , as displayed in Fig. 2(d). Contrary to the case of a fresh junction, shown in Figs. 1–3, the channel current under the negative gate voltage reached a maximum level, and then immediately dropped to a lower level. Furthermore, the current level dropped successively with the increase of bias voltage, i.e., larger channel current, for different  $V_g$  values. The photon energy of an UV source with wavelengths of 340 nm, used in this study, is 3.55 eV, which is high enough to break<sup>19</sup> the possible chemical bonds on the surface of CNT, such as

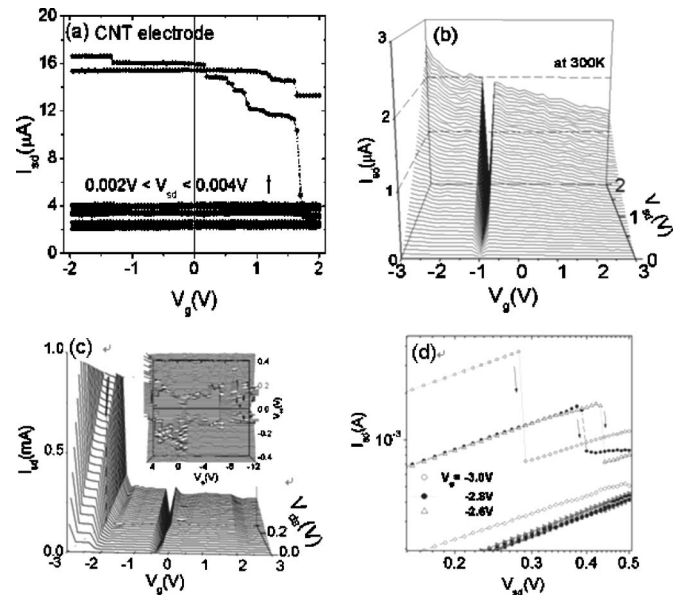


FIG. 2. (a) Gate response characteristics of the electrode of CNTs under small drain bias. (b) Gate response of CNT channel with drain bias level. (c)  $I$ - $V_g$  characteristics after UV exposure. (d) Conductance contour as a function of  $V_{sd}$  and  $V_g$  obtained at 9 K. The figures show the electrical breakdown of the high current carrying CNT channels under continuous electrical stressing.

the C–H bond (3.5 eV), O–H bond (4.44 eV), H–H bond (4.52 eV), and the C–C (6.29 eV) bond of CNTs if multiphoton excitation occurs. So,  $I_{sd}$  in our device could be enhanced by the cleaning effect of the surface. Also, the drop of channel current level at fixed negative  $V_g$  was only seen in the suspended junction where the CNT was treated by low intensity UV light, and the drop in  $I_{sd}$  after UV irradiation indicated the possible peeling or rupture of an insulated or contaminated portion at higher channel current. A similar kind of the electrical breakdown based on a different mechanism on the CNT under high bias was reported by Bourlon *et al.* and Dai group. The former reported that the outermost removed shell in direct contact with air and thus most subjected to rapid oxidation initiated by the current was responsible for the current drop, whereas Dai group addressed that electrical breakdowns occurred at a low bias for long channel of  $3 \mu m$  suspended CNT with Pd contacts due to joule heating resulting from the electron-optical phonon coupling and oxidation in air. The dramatic increase of current level to milliamper level and abrupt drops above a specific voltage indicate that the electrode CNT containing both amorphous carbon tubes and CNT may have experienced the cleaning effect due to UV light and/or oxidation and subsequently have broken down in air after UV treatment. Considering the fact that the larger diameter shells of multiwalled CNTs contribute more to channel current than the smaller ones, the current drop may be in partial due to the peeling in the channel CNTs. In the effective peeling after UV exposure, UV acted as a cleaning agent on the surface of the CNT, and thus the outmost CNT shell was easily exposed to air, providing no coverage of the amorphous carbon, etc.

Finally, to study the interface dipole effect between contact and CNT channel, we performed capacitance ( $C$ ) measurements by applying bias ( $V_{sd}$ ) between drain and source CNT electrodes. All data were collected in the ambient and under ambient lighting by using the HP impedance analyzer

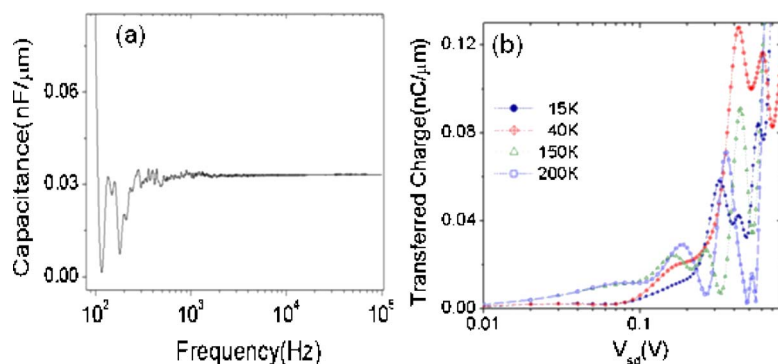


FIG. 3. (Color online) (a) Capacitance ( $C$ ) vs frequency ( $f$ ) characteristics for the CNT channel of all-CNT-based junction measured at room temperature and (b) transferred charge ( $Q$ ) (estimated from capacitance measurement) vs  $V_{sd}$  as a function of temperature. During the measurements, ac voltage was applied between drain and source.

(HP model 4192). Figure 3(a) shows the impedance spectra of a suspended CNT channel from 100 Hz to 100 kHz. When the frequency of 1 mV oscillation level was swept, the initial high capacitance in the low frequency regime dropped abruptly, and oscillations were observed up to a few kilohertz regime and finally above a few kHz, the oscillations of capacitance maintained at fixed capacitance value. At very low frequencies below 100 Hz, the capacitance, which corresponded to the ac analogy with the  $I_{sd}$  under  $V_{sd}$  was very high. According to the Zhao *et al.*, in the low frequency range ( $<100$  kHz), a very long channel CNT with  $\text{SiO}_2$  gate insulators showed the total capacitance of about  $600 \text{ pF}/\mu\text{m}$  ( $6 \text{ nF}/10 \mu\text{m}$  in the literature<sup>20</sup>), whereas in our case, the capacitance was about  $35 \text{ pF}/\mu\text{m}$ , which was much lower than that of the metal (i.e., tungsten)-CNT-metal (i.e., tungsten) junction. The reduction of capacitance in our junction is ascribed to both the continuity of material and structure, i.e., CNT electrodes–CNT channel–CNT electrode junction, made by direct *in situ* growth and clean interface. Also, Fig. 3(b) shows the spectra of transferred charge ( $Q=C/V_{sd}$ ) versus voltage. The junction shows temperature independent behavior below  $V_{sd}=7 \text{ mV}$ , then near the higher  $V_{sd}$  region, the capacitance of the junction at 9 K temperature is higher than that at 295 K. We suggest that this decreased transferred charge ( $Q$ ) at lower bias and wider depleted region at bias axis indicate a Coulomb blockade behavior observed in dc  $I$ - $V_{sd}$  measurement in the lower temperature regime [inset in Fig. 3(c)] and furthermore, capacitance spectroscopy on planar configuration can provide a feasible analysis tool for the CNT junction.

As a summary, we have demonstrated suspended all-CNT-based field effect transistor not only to maintain continuity of interface between electrode and channel but also to provide a more easy construction method for CNT junction by introducing a designed diluted catalytic metal-doped multilayered film. Our suspended CNT channel with the entangled CNTs as contact electrodes showed ambipolar transistor behavior, displaying nearly the same barrier height for the hole and electron conduction. Also, the current level was changed by low intensity UV treatment, resulting in a high conductive channel that shows more *P*-type dominant behavior. Furthermore, we introduced capacitance ( $C$ ) versus frequency (voltage) characteristics, which show the release of carriers from the CNT channel like as dc  $I$ - $V$  results at low

temperature regime. With more scalable processes and optimized properties, the unified structure of this virtual CNT electrode–CNT channel–virtual CNT electrode made by using a well-designed catalyst may contribute to the simplest and most cost effective realization of nanoelectrospin devices and provide model building blocks for gate-controlled devices.

The authors thank J. H. Kim, J. A. Lee, Y. M. Kim, I. W. Park, and K. J. Song for their help during the experiments. This work was supported by the Nano Basic Technology Project, National Research Laboratory Program of the KOSEF in Korea and partially, KRF project [KRF-2005-C00054 (I00183)] and BK21.

- <sup>1</sup>S. J. Tans, A. R. M. Verschueren, and C. Dekker, *Nature (London)* **393**, 49 (1998).
- <sup>2</sup>A. Javey, H. Kim, M. Brink, Q. Wang, A. Ural, J. Guo, P. McIntyre, P. McEuen, M. Lundstrom, and H. Dai, *Nat. Mater.* **1**, 242 (2002).
- <sup>3</sup>A. Javey, J. Guo, Q. Wang, M. Lundstrom, and H. Dai, *Nature (London)* **424**, 654 (2003).
- <sup>4</sup>M. Freitag, Y. Martin, J. A. Misewich, R. Martel, and Ph. Avouris, *Nano Lett.* **3**, 1067 (2003).
- <sup>5</sup>F. Leonard and J. Tersoff, *Phys. Rev. Lett.* **84**, 4693 (2003).
- <sup>6</sup>Y. Xue and M. A. Ratner, *Phys. Rev. Lett.* **70**, 205416 (2004).
- <sup>7</sup>Y. Yaish J.-Y. Park, S. Rosenblatt, V. Sazonova, M. Brink, and P. L. McEuen, *Phys. Rev. Lett.* **92**, 046401 (2004).
- <sup>8</sup>N. Park and S. Hong, *Phys. Rev. B* **72**, 045408 (2005).
- <sup>9</sup>Yongqiang Xue and Mark A. Ratner, *Phys. Rev. B* **69**, 161402 (2004).
- <sup>10</sup>S. J. Wind, J. Appenzeller, and Ph. Avouris, *Phys. Rev. Lett.* **91**, 058301 (2003).
- <sup>11</sup>K. Alam and R. K. Lake, *J. Appl. Phys.* **98**, 064307 (2005).
- <sup>12</sup>S. Heinze, J. Tersoff, R. Martel, V. Derycke, J. Appenzeller, and Ph. Avouris, *Phys. Rev. Lett.* **89**, 106801 (2002).
- <sup>13</sup>H. J. Li, W. G. Lu, J. J. Li, X. D. Bai, and C. Z. Gu, *Phys. Rev. Lett.* **95**, 086601 (2005).
- <sup>14</sup>Yun-Hi Lee, Y. T. Jang, J. H. Ahn, and B. K. Ju, *Adv. Mater. (Weinheim, Ger.)* **13**, 1371 (2001).
- <sup>15</sup>Yun-Hi Lee, Je-Min Yoo, J. A. Lee, S. Y. Ahn, J. Joo, S. Lee, B. K. Ju, and K. J. Song, *Appl. Phys. Lett.* **87**, 121915 (2005).
- <sup>16</sup>J. Appenzeller, M. Radosavljevic, J. Knoch, and Ph. Avouris, *Phys. Rev. Lett.* **92**, 048301 (2004).
- <sup>17</sup>R. J. Chen, N. R. Franklin, J. Kong, J. Cao, T. W. Zhang, and H. Dai, *Appl. Phys. Lett.* **79**, 2258 (2001).
- <sup>18</sup>Moonsub Shim, Ju Hee Back, Taner Ozel, and Kwan-Wook Kwon, *Phys. Rev. B* **71**, 205411 (2005).
- <sup>19</sup>Y.-P. Zhao, B. Q. Wei, P. M. Ajayan, G. Ramanath, T.-M. Lu, G. C. Wang, A. Rubio, and S. Roche, *Phys. Rev. B* **64**, 201402 (2001).
- <sup>20</sup>W. J. Zhao, N. Kawakami, A. Sawada, and M. Takai, *J. Vac. Sci. Technol. B* **21**, 1734 (2003).